Projecting Permafrost Thaw of Sub-Arctic Tundra With a Thermodynamic Model Calibrated to Site Measurements

A. Garnello[1,2] , S. Marchenko[3], D. Nicolsky[3] , V. Romanovsky[3] , J. Ledman[1,2], G. Celis[4], C. Schädel[1,2] , Y. Luo[1,2] , and E. A. G. Schuur[1,2]

[1]Center for Ecosystem Science for Society, Northern Arizona University, Flagstaff, AZ, USA, [2]Department of Biological Sciences, Northern Arizona University, Flagstaff, AZ, USA, [3]Geophysical Institute, University of Alaska Fairbanks, Fairbanks, AK, USA, [4]Agronomy Department, University of Florida, Gainesville, FL, USA

Abstract Northern circumpolar permafrost thaw affects global carbon cycling, as large amounts of stored soil carbon becomes accessible to microbial breakdown under a warming climate. The magnitude of carbon release is linked to the extent of permafrost thaw, which is locally variable and controlled by soil thermodynamics. Soil thermodynamic properties, such as thermal diffusivity, govern the reactivity of the soil-atmosphere thermal gradient, and are controlled by soil composition and drainage. In order to project permafrost thaw for an Alaskan tundra experimental site, we used seven years of site data to calibrate a soil thermodynamic model using a data assimilation technique. The model reproduced seasonal and interannual temperature dynamics for shallow (5–40 cm) and deep soil layers (2–4 m), and simulations of seasonal thaw depth closely matched observed data. The model was then used to project permafrost thaw at the site to the year 2100 using climate forcing data for three future climate scenarios (RCP 4.5, 6.0, and 8.5). Minimal permafrost thawing occurred until mean annual air temperatures rose above the freezing point, after which we measured over a 1 m increase in thaw depth for every 1 °C rise in mean annual air temperature. Under no projected warming scenario was permafrost remaining in the upper 3 m of soil by 2100. We demonstrated an effective data assimilation method that optimizes parameterization of a soil thermodynamic model. The sensitivity of local permafrost to climate warming illustrates the vulnerability of sub-Arctic tundra ecosystems to significant and rapid soil thawing.

Plain Language Summary Across Arctic environments, cold temperatures maintain perennially frozen ground, which store ancient carbon from dead plants. Climate warming is thawing this ground, potentially transferring carbon from the soil into the atmosphere, further contributing to planet warming. How this ground thaws varies across the landscape due to complex soil properties. We created a model for predicting how much the ground would thaw by 2100. This model used seven years of measurements made at an Alaskan tundra research site near Denali Park for calibration. The model was accurate over this seven-year period, producing results which closely match our observed data. Our model showed that over 1 m of ground is expected to thaw for every 1 °C sustained rise in air temperature, leading to 5–13 m of ground thawing to occur by 2100, dependent on the extent of air warming. This result demonstrated a novel method for obtaining precise local estimates of ground thawing that rely on site measurements and highlights the extreme vulnerability of Arctic ground to thawing in the face of climate change. This study is important because it allows for local predictions of Arctic ground thawing, which are a key component for the full extent of soil carbon loss into the atmosphere.

1. Introduction

The thawing of permafrost soils across the Arctic illustrates the age of contemporary climate warming (Åkerman & Johansson, 2008; M. T. Jorgenson et al., 2010; Osterkamp & Romanovsky, 1999; Romanovsky et al., 2008; Serreze et al., 2000). Previously, frozen soil carbon becomes accessible to microbial decomposition when thawed (Keuper et al., 2012; Mack et al., 2004; van Huissteden & Dolman, 2012), exposing a pool between 1460 and 1600 Pg of soil carbon (Cavallaro et al., 2018; Koven et al., 2013; E. A. G. Schuur et al., 2008, 2009; Tarnocai et al., 2009). The Arctic permafrost soil carbon pool constitutes nearly double the amount of carbon currently in the atmosphere, reinforcing the need for precise estimates of future permafrost thaw. Further, knowing the degree to which soil column temperatures will rise is a key part

of estimating the vulnerability of thawed permafrost soil carbon to microbial decomposition (Davidson & Janssens, 2006; Parmentier et al., 2017).

Despite efforts to integrate permafrost thaw dynamics into earth systems' models, projections of thaw extent vary widely due to differing model representation of Arctic soil regimes and their past climate histories (Koven et al., 2013; McGuire et al., 2016; Olefeldt et al., 2016; Slater & Lawrence, 2013). This variability can, in part, be attributed to different representation of freezing and thawing processes, snow insulation effects, and differences in estimated soil thermodynamic properties in different models (Zhu et al., 2019). Soil thermodynamic properties, such as diffusivity, govern the reactivity of the soil-atmosphere thermal gradient, and are controlled by soil composition, temperature, and water content. Given the highly variable nature of these soil components across the discontinuous permafrost zone, coarse representation of soil column structure and composition will often fail to represent local sites, as has been seen in site-model intercomparison studies (Schädel et al., 2018). Furthermore, precise estimation of soil thermodynamic properties is often a barrier to site-calibration of soil models, despite being the best option for obtaining a locally representative projection of permafrost thaw.

Site-calibrated modeling is an effective means for characterizing systems with unique thermodynamic properties (Romanovsky & Osterkamp, 2000; Romanovsky et al., 2007). For example, soil structures within the discontinuous permafrost zone are consistently misrepresented at larger spatial scales, owing to high spatial variability of permafrost, soil organic layer, and plant community composition. Earth systems' models disagree widely on the maximum mean annual air temperature at which permafrost occurs, underscoring the utility of locally calibrated models for Arctic sites with mean annual air temperatures near 0 °C (Koven et al., 2013). While Earth systems' models are effective tools for visualizing patterns on a broad scale, they will inherently fail to represent a highly localized system without requiring detailed re-parameterization efforts (Luo & Schuur, 2020). Indeed, locally calibrated models should remain a viable tool for characterization of highly vulnerable areas as informative comparisons with landscape models and as a valuable tool for their benchmarking.

Regions along the southernmost permafrost boundary are particularly vulnerable to changing climate. Long-term soil temperature records of permafrost across Alaska have confirmed a prolonged warming trend since the mid-1980s, narrowing most discontinuous permafrost temperatures to −2 °C or warmer at zero amplitude depth (Romanovsky et al., 2017, 2010). Statewide projections of near-surface permafrost persistence in a warmer climate demonstrate widespread loss of Tundra permafrost, predominantly along the southern Alaskan boundary by 2050 (Jafarov et al., 2012; Pastick et al., 2015). The landscape subsidence and thermokarst formation following ice-rich soil thawing can drive state-changes in ecosystem carbon fluxes (Aalto et al., 2018; Natali et al., 2011; E. A. G. Schuur et al., 2007) and costly damages to civil infrastructure (Hjort et al., 2018). Furthermore, studies on the impending thaw of sub-Arctic permafrost zones inform on the future state of currently relatively stable continuous permafrost.

This experiment explored the vulnerability of sub-Arctic tundra permafrost to thawing under projected climate change. Through a data assimilation method involving a multi-year vertically explicit soil temperature time series, we provide a framework for producing a locally calibrated model. Our questions in this experiment are (1) What is the immediate and long-term fate of permafrost at a sub-Arctic tundra experimental site? and (2) How effective is this data assimilation technique at locally calibrating a soil heat model? This experiment utilized the Geophysics Institute Permafrost Laboratory model 2.0 (GIPL) (Jafarov et al., 2012; Marchenko et al., 2008), which is a numerical heat model focusing on the thermodynamic properties of individual soil layers. Our data assimilation approach treated GIPL parameter values as distributions, as opposed to static values, iteratively generated through model inversion. Therefore, parameter value distributions were the sole driver of model uncertainty and were used to assess confidence in our representation of the site soil column. GIPL parameter estimates, simulated ground temperature, active layer thickness, and associated uncertainty were used to assess method effectiveness. Three separate forecasts from the Coupled Model Intercomparison Project, Phase 5 (CMIP5) corresponding to future climate scenarios were used to drive the calibrated model to 2100, where permafrost thaw vulnerability to varying degrees of air warming were investigated on site.

2. Materials and Methods

2.1. Experimental Site

Eight Mile Lake experimental thaw gradient site (63°52′42.1′N, 149°15′12.9′ W) is located in the northern foothills of the Alaska range, just outside Denali National Park (E. A. G. Schuur et al., 2007). This area is classified as moist acidic tundra, and with a plant community composition dominated by the tussock-forming sedge *Eriophorum vaginatum* and the deciduous shrub *Vaccinium uliginosum* (Natali et al., 2011). The soils are Gelisol, with a 0.25 m thick organic horizon overlaying cryoturbated mineral soils, with permafrost consistently within 1 m of the surface. The longterm mean air temperature at Eight Mile Lake is −1 °C from 1976 to 2009, with monthly-average air temperature ranges between −16 °C (December) and 15 °C (July) (National Climatic Data Center, NOAA). The permafrost at the Eight Mile Lake is classified as climate-driven and ecosystem protected (Shur & Jorgenson, 2007), demonstrating the strong insulating effects of the organic layer preventing rapid thawing during warm summer months.

Eight Mile Lake exhibits a natural gradient of permafrost thaw which occurred over recent decades. Thermokarst features comprise nearly 12% of the watershed (Belshe et al., 2013), and shrub-dominated tundra terrain continues to expand over graminoid-tundra areas with increased soil drainage (E. A. G. Schuur et al., 2008). The Eight Mile Lake tundra ecosystem is typically a carbon source to the atmosphere due to strong soil respiration signals over the growing season and winter (Celis et al., 2017); however this carbon source strength is highly dependent on inter-seasonal variability. Long-term monitoring of deep permafrost temperatures at Eight Mile Lake have shown a gradual warming since 1986 of nearly 0.5 °C at 25 m depth between 1986 and 2003 (Osterkamp et al., 2009; Osterkamp & Romanovsky, 1999), and a more recent warming of approximately 0.1 °C between 9 and 26 m from 2007 to 2017 (Romanovsky et al., 2020). Radiocarbon analyses of the soil respiration signal link the deepening of the permafrost boundary at Eight Mile Lake to a 6%–18% increase in proportion of old soil carbon respiration in recent decades (Pries et al., 2012). These analyses have demonstrated high confidence in climate warming increasing the ecosystem carbon source strength, respiration of old soil carbon, and permafrost temperatures of Eight Mile Lake. Given the extensive history of site measurements, the comparability of this site to other areas of tundra throughout the discontinuous permafrost zone, and the particular vulnerability of warm discontinuous permafrost to thawing, this research site was an ideal choice for a locally-calibrated permafrost thaw projection.

Seven years (2012–2018) of climatological and vertically-resolved soil temperature data from the Eight Mile Lake experimental research site (Celis et al., 2019) was used to calibrate the Geophysical Institute Permafrost Laboratory 2.0 model (GIPL). Daily aggregated temperatures at 5, 10, 20, and 40 cm depths measured at 30 min intervals by type-T thermocouples controlled by a CR10X and CR1000 datalogger (Campbell Scientific, Logan, Utah) were used as model calibration and evaluation data for shallow soil layers. For calibration and model evaluation of deeper soil layers, annual temperature measurements from a nearby permafrost borehole at 2, 4, 8, and 15 m were included in the soil temperature data (Osterkamp & Romanovsky, 1999). This borehole is located approximately 80 m south from the vegetation monitoring plots where the shallow temperature series are measured and encompasses highly corresponding soil and vegetation conditions. In addition, mean biweekly growing season thaw-depth probe measurements were taken across vegetation monitoring plots to represent seasonal thaw dynamics (Kelley et al., 2019). The number of plots available for biweekly seasonal thaw depth vary by year (from $n = 3$ to $n = 15$). These measurements do not account for intra-season thaw subsidence, which has been estimated at a nearby experimental site as ∼5 cm between May and August (Rodenhizer et al., 2020). Furthermore, between 2011 and 2018 annual thaw subsidence was estimated at approximately 1 cm per year (Rodenhizer et al., 2020). Hourly air temperature (°C) was measured using an Onset HOBO (Bourne, MA) (Celis et al., 2016), and hourly snow depth data (Ledman et al., 2018) measured using a rugged acoustic sensor through an SR50A datalogger (Campbell Scientific, Logan, Utah) and were both aggregated to mean daily values (Figure 1).

Nearly 40% of the daily snow-depth timeseries was gap-filled using meteorological variables collected onsite, including air temperature, incoming radiation, and snow-depth values measured at another experimental site located approximately two miles west. The model resulted in an average daily snow-depth error of 4.5 cm during periods of snow cover.
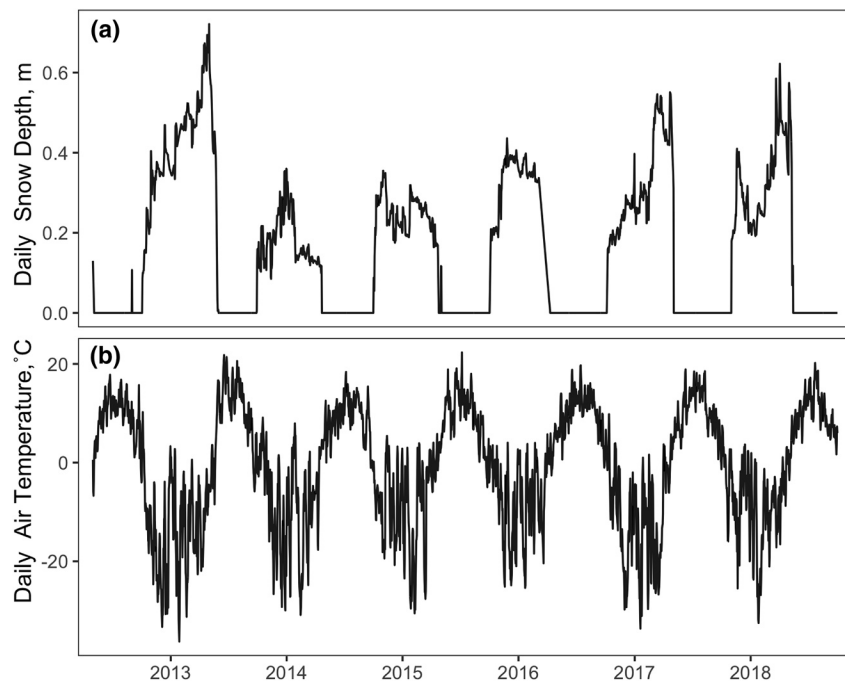
Figure 1. Measured climate variables over the calibration period (2012–2018) at the Eight Mile Lake research site. Daily average snow depth measured only during periods of snow (a). Daily average air temperature (b).

2.2. Soil Heat Model and Optimization Method

We simulated site soil temperature dynamics using the GIPL (Nicolsky et al., 2009, 2007), which calculates seasonal thawing and freezing using 1D nonlinear heat equations, including the phase change of water throughout the soil column. The GIPL conserves energy within the soil column, with the upper boundary condition set by the surface air temperature and snow-pack thermal dynamics, and the bottom boundary at 100 m representing bedrock with a geothermal heat flux of 0.021234 °C/m. The GIPL requires daily air temperature and snow depth as climatic drivers and includes a built-in modeling framework of snow density (Verseghy, 1991) which is used to calculate snowpack insulator effects. A higher density snowpack is seen by the GIPL as a less efficient insulator of the soil surface. Each individual soil layer contains eight prescribed thermodynamic parameters (Table 1) that remain static through individual simulations. These parameters, when combined with the climatic drivers, are used to produce a daily temperature distribution along the soil column and will be the focus of stochastic algorithm optimization methods.

Table 1
GIPL Model Parameters Definitions, and Their Prior Ranges for the MCMC Optimization Method Defined by Soil Layer Organic Category

Parameter name	Unfrozen water curve coefficients	Volumetric water content	Thermal conductivity (thawed material)	Thermal conductivity (frozen material)	Volumetric heat capacity (thawed material)	Volumetric heat capacity (frozen material)	Layer depths
Model definition	a,b,c	η	λ_t	λ_f	C_t	C_f	–
Parameter units	Coefficients (unitless)	m/m	W/(m*K)	W/(m*K)	J/(m^{3}K) * e7	J/(m^{3}K) * e7	–
Organic layer	–	[0.10, 0.75]	[0.1, 1.5]	[0.45, 1.9]	[1.25, 2.3]	[0.5, 1.5]	0–40 cm
Organic/mineral layer	–	[0.10, 0.75]	[0.8, 1.9]	[1.1, 2.3]	[1.05, 2.0]	[0.35, 1.3]	41–98 cm
Silt/mineral layer	–	[0.10, 0.75]	[1.1, 2.2]	[1.35, 2.6]	[0.85, 1.8]	[0.35, 1.3]	99 cm–15 m

Note. Values inside brackets represent [minimum, maximum] of the uniform prior range interval. For parameter units: m = meters, K = degrees Kelvin, J = Joules.

In order to accurately simulate temperature along a soil column, the GIPL allows for distinct soil thermodynamic properties attributable to depths along a soil column which differ in their organic and structural properties. This experiment defined 11 distinct soil layers, with lower boundaries existing at 3, 8, 19, 41, 56, 76, 99, 305, 513 cm, 15 m, and a bottom boundary at 100 m which we determined from site familiarity, analysis of soil cores, available temperature data, and model restrictions. Soil cores drilled down to 5 m characterize these upper layers as highly organic near the surface with gradually increasing silt and gravel inclusions between 1 and 5.5 m. A 30 m temperature core drilled described the 5.5–30 m section of permafrost as containing gravel, boulders, and underlain by sand (Osterkamp et al., 2009). Given a limited number of layers available to the GIPL model, we prioritized differentiating soil layers in the upper 1 m of the soil column and assigned static thermodynamic properties to the 15–100 m soil layer using the characteristics provided by Osterkamp et al., (2009) and estimated the thermal property values of Nenana Gravel using Kersten (1949). No bedrock data was available; therefore no assumptions of bedrock formation within the top 100 m were made. Further, since observed temperature change at these deep layers occurs on decadal timescales, estimates of parameter values for these layers using this method would yield highly uncertain results.

The posterior distribution of GIPL soil layer parameters were estimated using a Markov chain Monte Carlo (MCMC) method (Andersen et al., 2003). This method relies on Bayes Theorem, where the posterior distribution of model parameters for a set of observations are proportional to a likelihood function (see Equation 1) and their prior distributions. This parameterization approach is a novel diversion from traditional steepest-descent methods (Nicolsky et al., 2009) which explores the utility in measured data to provide accurate model parameters instead of manual user-input. A full description of this method can be found in Xu et al. (2006). First, a prior probability density function was specified for each GIPL parameter across specified soil layers. This was specified as a uniform distribution over intervals determined through a combination of literature values, accumulated knowledge about the site, and previous model runs (Farouki, 1981; Kersten, 1949; Nicolsky et al., 2009) (Table 1).

Equation 1, Likelihood Function:

$$P\left(Z \mid c\right) \propto exp\left\{-\sum_{i=1}^{11}\frac{1}{2\sigma_i^2}\sum_{t\in obs\left(Z_i\right)}^{2,345}\left[Z_i\left(t\right)-\varphi_i X\left(t\right)\right]^2\right\} \tag{1}$$

$P(Z|c)$ stands for the likelihood function, $Z_i(t)$ is the measured temperature at time t, for soil layer Z_i, and $\varphi_i X(t)$ being the modeled temperature value for layer i, at time t, and σ being error associated with each measurement. σ was determined individually for each layer i according to typical disagreement observed for matching soil layers across nearby monitoring plots (Table S2).

Within these intervals, parameter value space was sampled with an adaptive Metropolis-Hastings algorithm (Metropolis et al., 1953). Iteratively, a set of candidate parameter values were proposed, and accepted on the condition of satisfying the Metropolis criterion Equations 2a and 2b (Spall, 2003)

$$P\left(c^{(k-1)}, c^{new}\right) = min\left\{1, \frac{L\left(c^{new}\right)q(c^{(k-1)} \mid c^{new})}{L\left(c^{new}\right)q(c^{new} \mid c^{(k-1)})}\right\} \tag{2a}$$

$$c^k = c^{new} \mid P\left(c^{(k-1)}, c^{new}\right) \geq U \tag{2b}$$

The Metropolis criterion: The probability of a proposed parameter value (c^{new}) following the previously accepted parameter value ($c^{(k-1)}$) is the minimum between the value of 1, and a comparison of the targeted stationary distributions $L(c)$ (also known as $P(c|Z)$) and proposal distributions $q(c^{new}|c^{(k-1)})$. Then, $P\left(c^{(k-1)}, c^{new}\right)$ is compared to a random number, U from the uniform distribution $U[0, 1]$ defined on the

interval [0, 1]. The proposed parameter value c^{new} is accepted under the conditions that $P\left(c^{(k-1)}, c^{new}\right)$ is $\geq U$ (Table S2).

Equation 2a simplifies into $min\{1, >1\}$ when the proposed parameter c^{new} yields a decreased model error than the previously accepted parameter $c^{(k-1)}$, which sets $P\left(c^{(k-1)}, c^{new}\right)$ equal to 1. According to Equation 2b, when $P\left(c^{(k-1)}, c^{new}\right)$ is equal to 1, the proposed parameter c^{new} will be accepted. When c^{new} yields a larger model error than $c^{(k-1)}$, $P\left(c^{(k-1)}, c^{new}\right)$ becomes the output of Equation 2a, with this value being proportional to the magnitude cost increase yielded by c^{new}. Values of c^{new} which cause a relatively large increase in model error yield lower relative values of $P\left(c^{(k-1)}, c^{new}\right)$, which will pass the test criterion of Equation 2b less frequently. Thus, the Metropolis criterion accepts worse parameter sets in a proportion to how much the proposed parameter set increases model error.

The Metropolis-Hastings algorithm was employed to construct the stationary posterior distribution of each parameter, which was then sampled to create the Markov chain for recreation and projection of soil temperature and permafrost thaw. The full series of measured temperature and thaw values for shallow and deep soil layers were used as calibration data for model parameterization as well as for model evaluation.

The union of five parallel Markov chains was used to determine the final posterior distributions of the parameter space. Five chains were constructed to ensure that an acceptable range of initial values across each prior was achieved, and to provide an adequate number of chains with which to test for proper convergence. Each MCMC run began with parameter values dispersed at initial points across the prior distribution intervals and was simulated 150,000 times. With a model simulation acceptance rate near 30%, each finished Markov chain yielded approximately 40,000 parameter values. The first half of the accepted iterations for each run were discarded as the burn-in period, yielding approximately 100,000 parameter sets used for analysis. Convergence of the five chains to the stationary distribution was tested using the Gelman-Rubin diagnostic (Gelman & Rubin, 1992). The results of the Gelman-Rubin diagnostic showed upper confidence values for each parameter under 1.09, and an overall potential scale reduction factor of 1.09, indicating proper convergence of each chain, and on each parameter. These analyses were done using the CODA package in R (Plummer et al., 2006; R Core Team, 2019).

Of the 88 possible parameters (11 layers by 8 parameters), only 48 were included in the optimization method. These included the volumetric water content η, thermal conductivity λ_f, and volumetric heat capacity C_f of the soil while under frozen conditions for the upper 15 m, and the thermal conductivity λ_t and volumetric heat capacity C_t for the soil under thawed conditions for the upper 99 cm (Table 1). Certain parameters were excluded from the cost function if there were no representative site data available for model verification. For example, we did not observe thawing of soil below 1 m, therefore only the frozen soil parameters below 1 m were included in the cost function. Thus, the thermal capacity and conductivity for the thawed soil component of deep layers were prescribed according to the proportion of frozen/thawed capacity and conductivity of accepted parameters for the 76–99 cm soil profile. We excluded the parameters behind the unfrozen water content curve function from the Bayesian inversion, choosing to manually prescribe their values near literature values based on the mineral and organic composition of the layers. As freezing temperatures move down the soil column, sub-zero temperatures cannot propagate through a soil layer until the water molecules turn to ice. The rate at which these temperatures drive liquid water freeze-up is what the unfrozen water content parameters control. These parameters were excluded from the parameterization method due to their high nonlinearity in relation to the other parameters - their inclusion in the parameterization method prevented convergence of the MCMC chains and prohibited consistent covariance matrix construction, a requisite for how parameter sets were generated after the burn-in period. The GIPL does not differentiate excess water in a soil layer that is not absorbed by the natural porosity of the unfrozen material.

We performed subsequent sensitivity tests comparing projections of permafrost thaw depth at 2100 constructed using a different range of values for the unfrozen water content parameters. We selected another set of values which emphasized warming over the calibration period of the permafrost layers to see the sensitivity of model projections to these parameter values. These new values led to a 16% (2.2 m) increase

in thaw depth by 2100 for RCP 8.5 (Figure S1, *Run B*), and a small relative difference for the other RCPs. Furthermore, another sensitivity test was conducted to see if model projections were strongly dependent on the time period used for the calibration. For this test, we implemented the optimization method for a calibration period which began in May 2013 and found only a 14% (or 2.1 m) increase in thaw depth by 2100 for RCP 8.5 (Figure S1, *Run C*). These tests were used to evaluate our confidence in the robustness of our model parameterization methods.

2.3. GIPL Application

We evaluated fit of the calibrated model by comparing model simulated temperature and thaw values to the measured data series. Five hundred accepted model parameter simulations were selected for further analysis to ensure that a representative estimate of simulation uncertainty of temperature series was captured. These sets were randomly selected from the output of the five parallel MCMC runs, and each was used to drive the GIPL over the calibration period. From these 500 simulations, the median and interquartile range (IQR) of daily temperature values for soil layers were extracted and compared with corresponding measured daily temperature series. The IQR highlights asymmetry in distributions and was therefore used to visualize uncertainty in model simulations. Additionally, the mean and standard deviations of the maximum seasonal soil thaw depth values for the five hundred simulations were extracted and compared with measured values.

We then projected local permafrost thaw to 2100 using the same five hundred parameter sets and modeled climate data. The Coupled Model Intercomparison Project Phase 5, Assessment Report 5 (CMIP5, AR5) Five Model Average monthly-average air temperature projections were extracted and averaged across the 1.5 km^2 surrounding the Eight Mile Lake site, and linearly interpolated to daily values from 2010 to 2100. Then, decadal-monthly-average snow-water-equivalent from the Community Climate System Model, as part of CMIP5, AR5, were extracted and averaged for 1.5 km^2 surrounding the Eight Mile Lake site (Littell et al., 2018) and linearly interpolated to daily values. The CMIP5 climatology data were selected due to the high spatial resolution and the proven accuracy of the SWE product to reproduce historical data at Alaskan snow telemetry (SNOTEL) sites (Littell et al., 2018). Further, the CMIP5 air temperature and SWE models were both downscaled to 771 m^2 using Parameter-elevation Regressions on Independent Slopes Model 1971–2000 climatology for the state of Alaska (Daly et al., 2002). To get snowpack depth from the snow-water-equivalent output, the PERMAMODEL was used, which uses an empirical algorithm to melt snow according to surface temperature and to increase snow depth according to additional precipitation (Brown et al., 2003). Both sets of climatic data were extracted for three representative concentration pathways (RCP 4.5, 6.0, and 8.5) to determine the range in trajectories of permafrost temperature and thaw extent at the site (Figure 2). Furthermore, the same five hundred parameter sets were applied to each of the CMIP5 climate forcing data visualize the effect of climate variability on projected permafrost thaw at our site (Figure S1). Climate forcing data are available from the Scenarios Network for Arctic Planning and include a downscaling process which utilizes PRISM climatology from 1971 to 2000 to emphasize Alaskan areas. The authors of the climate data did not provide a climatology product for RCP 2.6. We measured the IQR of the five hundred model simulations to capture the magnitude and direction of model uncertainty across each concentration pathway.

3. Results

3.1. Model Calibration

The resulting posterior distributions showed varying levels of constraint across GIPL parameters and depths (Figure 3). Distributions that appear relatively flat indicate an ill-constrained parameter value. These ill-constrained parameter values are highly variable across model simulations and often assume a range of values across their initial prior ranges. Moreover, distributions which show peaks indicate an increasingly constrained parameter value within the area of the peak. Well constrained parameter values were found to be highly influential in affecting model output. Generally, the thermal conductivity and capacity values were highly variable in the layers deeper than 19 cm depth, where the opposite pattern held for the volumetric water content. The distributions suggest that controls on soil column temperature stem largely from
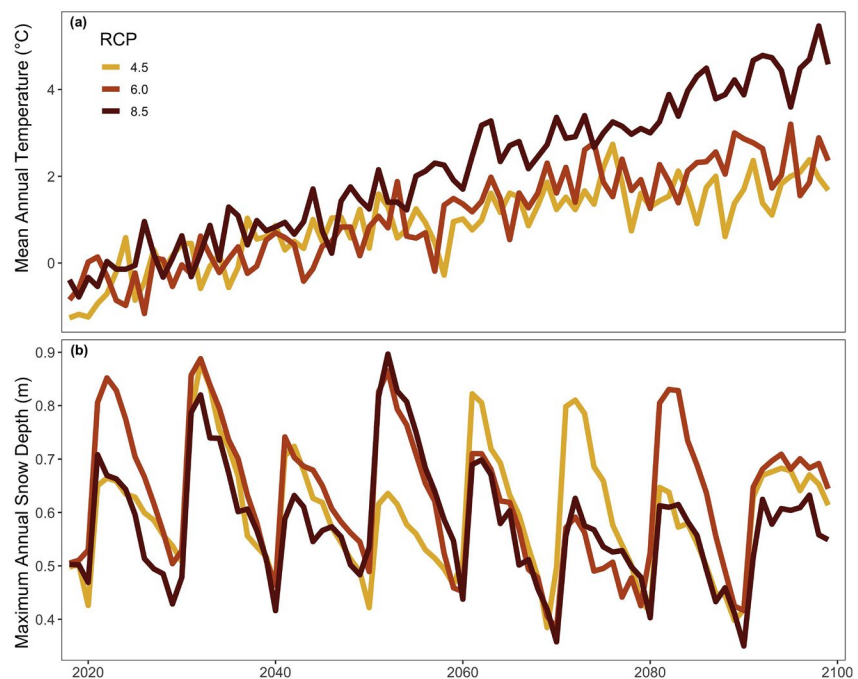
Figure 2. Annual projected climate variables for the Eight Mile Lake research site used to drive the calibrated GIPL model to 2100 for the three climate scenarios: 4.5 (yellow), 6.0 (orange), and 8.5 (red) using CMIP5, AR5 downscaled Alaska projections from 2018 to 2100. Mean annual air temperature from the CMIP5 5-model average (a). Maximum annual snow depth at the site calculated from snow-water-equivalent outputs of the CCSM4 modeled into snow depth using the PERMAMODEL (b).

near-surface layer conductivity and capacity, with volumetric water content becoming more influential with depth. While thermal conductivity and capacity throttle temperature flow across layers, the volumetric water content term controls, in part, how much energy is lost or gained from the phase change of water in individual layers. Due to the highly insulative property of the 3–19 cm layer, the amount of heat energy available to deeper layers is significantly reduced, thereby minimizing the effect of the thermal conductivity and capacity parameters to affect temperature change. Instead, where the magnitude of heat influx is relatively low, the interaction between volumetric water content and unfrozen water content terms drives temperature change. We attribute high variability for 3 cm parameters to the highly variable nature of surface soil, which experience a wider range of direct environmental pressures brought about from precipitation, seasonal changes in vegetation, and freeze/thaw dynamics. Also, it has been reported previously that relatively similar GIPL temperature fields can be generated from several different combinations of parameters (Beven & Freer, 2001; Nicolsky et al., 2007), suggesting that more detailed datasets would be needed to increase the parameter constraint.

3.2. Recreation of Eight Mile Lake Soil Thermal Regime Over the Calibration Period

Simulated soil temperatures captured seasonal and diurnal patterns of air temperature across soil layers, particularly in the shallow layers (Figure 4). Generally, the shallower soil layers were better fit by the simulation values than deeper layers, with the best fit layer depth being 5 cm ($R^2 = 0.90$) (Table 2). Large seasonal swings of temperature are modeled at the 200 cm layer, with observable decreasing amplitude simulated at the 800 cm layer. Owing to the once-annual measurements for these permafrost layers, we are unable to confirm the simulated seasonal amplitude signal, though the presence of seasonal signals on temperatures at these depths have been recorded in comparable permafrost areas (Romanovsky et al., 2010). The GIPL simulations showed a cooling between mid-2013 and mid-2016 for the permafrost down to 800 cm, a trend which is not matched by the observed data which was nearly 0.2 °C warmer for the 800 cm layer during that period. Measurements over the calibration period showed a warming of approximately 0.15 °C at 1500 cm, though model simulations showed an insignificant temperature trend through time.
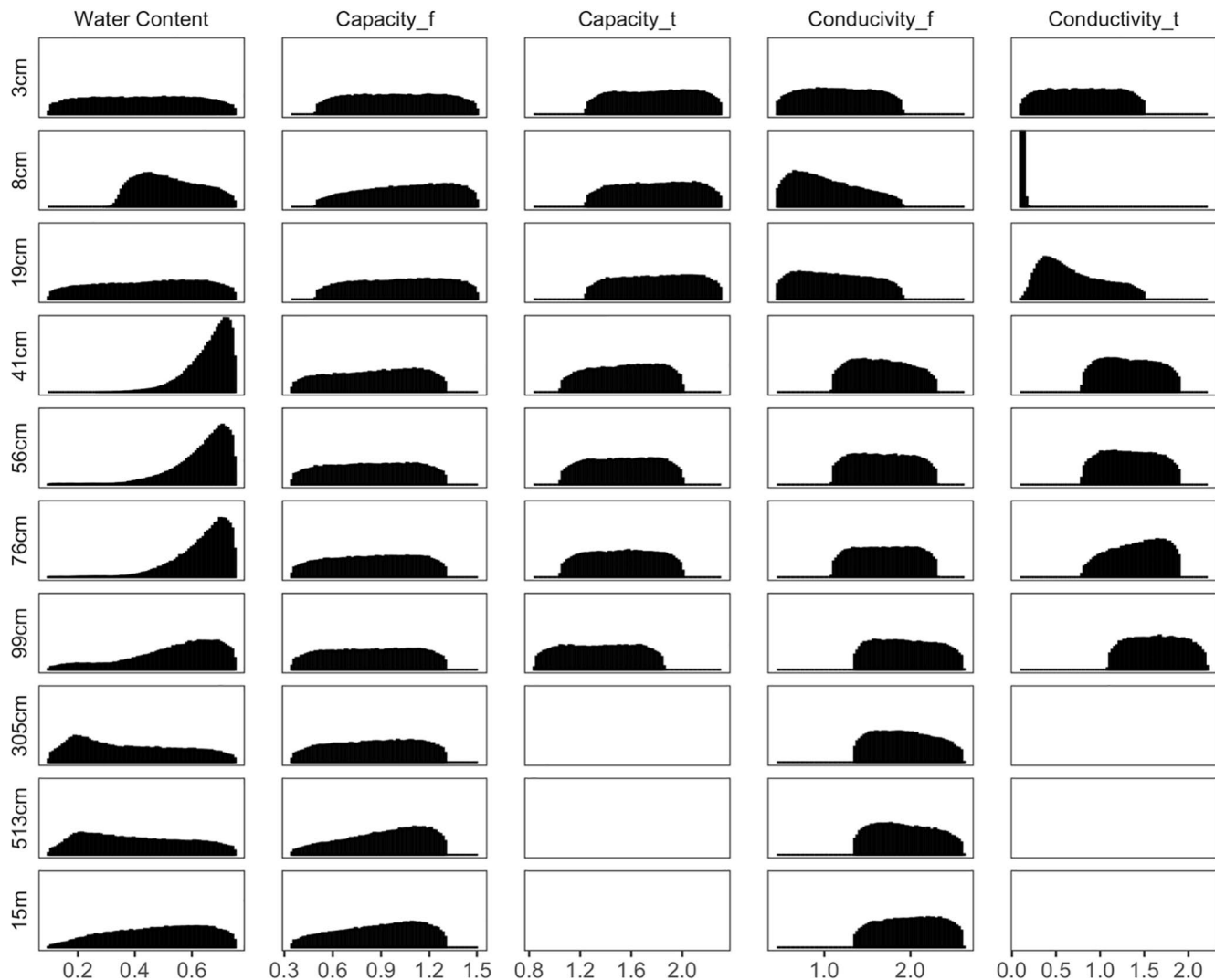
Figure 3. Frequency plot of the individual parameter posterior distributions for each depth, using the union of five parallel MCMC runs, approximately 100,000 iterations in total. *Rows* separate distributions by increasing soil depth. *Columns* separate counts across individual parameters (Table 1). Empty cells correspond to parameters left out of the cost function. *Note y-axis variable across plots to visualize shape of the distributions.*

Simulation divergence from observed soil temperatures was seasonally variable across depths. The model did a particularly poor job simulating October 2012 to May 2013 winter temperatures, with simulated temperatures colder than observed values by an average of 1.9 °C (+/−1.3 °C) for 5 cm, 1.69 °C (+/−1.1 °C) for 10 cm, and 1.3 °C (+/−1.08 °C) for the 20 cm layer (errors reported as standard deviations). Another similar divergence between model and observed appeared over the 2017–2018 winter period. Summertime model simulations were often colder than the observed series for the upper 40 cm layers, and the transitional seasons of spring and fall match more closely.

We used the width of simulation IQR to infer uncertainty of model representation of individual soil layers. Overall, the width of simulation IQR decreased with depth. The upper 10 cm demonstrated no strong seasonal pattern of IQR variability, with values consistently smaller than 1.5 °C (Figure S2). However, 20–40 cm layers demonstrated seasonal patterns in IQR variability, with a larger IQR window corresponding to periods of snow cover (January–April). However, the IQR series for these shallow layers displayed no overall trend through time, unlike the deep layers. The 200 and 400 cm layer IQRs spiked consistently during the later-Winter to early-Spring periods before gradually falling over the summer, corresponding to the periods of temperature transition from cooling to warming. The 800 and 1500 cm layers showed no strong
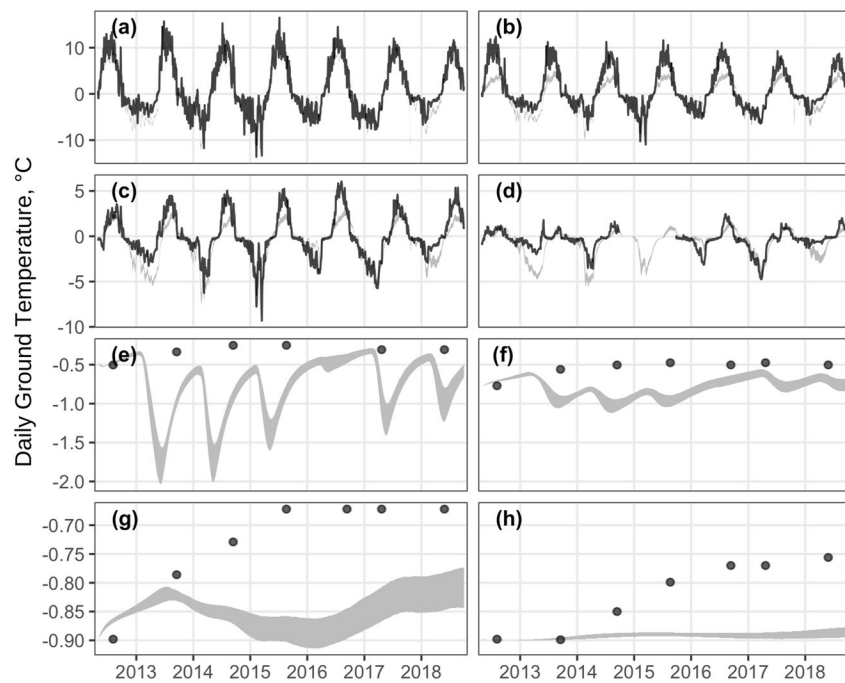
Figure 4. Measured and simulated daily mean ground temperatures across depths over the calibration period. Measured data is colored black, and simulated interquartile range is colored gray. *a–h* correspond to depths 5, 10, 20, 40, 200, 400, 800, and 1500 cm.

seasonal variability, however, these IQRs increased in range slightly between 2012 and 2018. The overall mean IQR for each temperature layer varied from 0.71 °C (10 cm) to 0.01 °C (1500 cm) (Table 2). Despite the observed uncertainty in parameter values, temperature simulations over the calibration period exhibit tight IQR ranges, providing confidence in model projections.

A critical element of permafrost table stability is the end of season thaw depth, which indicates the extent of top-down permafrost thawing which occurred for sites facing a deepening active layer. The average end of season thaw depth across multiple plots at the site between 2012 and 2018 measured 64.0 cm (+/−6.9 cm, standard deviation), while the simulation average end of season thaw depth was 65.2 cm (+/−3.9 cm, standard deviation) (Figure 5). The simulated versus empirical end of season thaw depths matched very well—all years had overlapping confidence intervals (Figure 5). The RMSE for end of season thaw depth between the median simulation and measured values was 4 cm (Table 2). For the plots used here, end of season thaw depth approximates the permafrost table depth.

3.3. Projecting Local Permafrost Thaw

Model simulations project soil column warming through 2100 across all RCP scenarios (Figure 6). As the degree of air warming increased, so did the width of the IQR for model simulations. After 2075, the IQRs for permafrost temperature projections above 800 cm were non-overlapping for RCP 8.5, demonstrating strong confidence in model simulations for these layers. Furthermore, thawing of the permafrost at the permafrost table is projected at the site for each RCP scenario (Figure 7). Median thaw depth surpasses 3 m by 2080, 2076, and 2061 for RCPs 4.5, 6.0, and 8.5, respectively, while by 2100 the range of median depths of the permafrost table is projected to be between
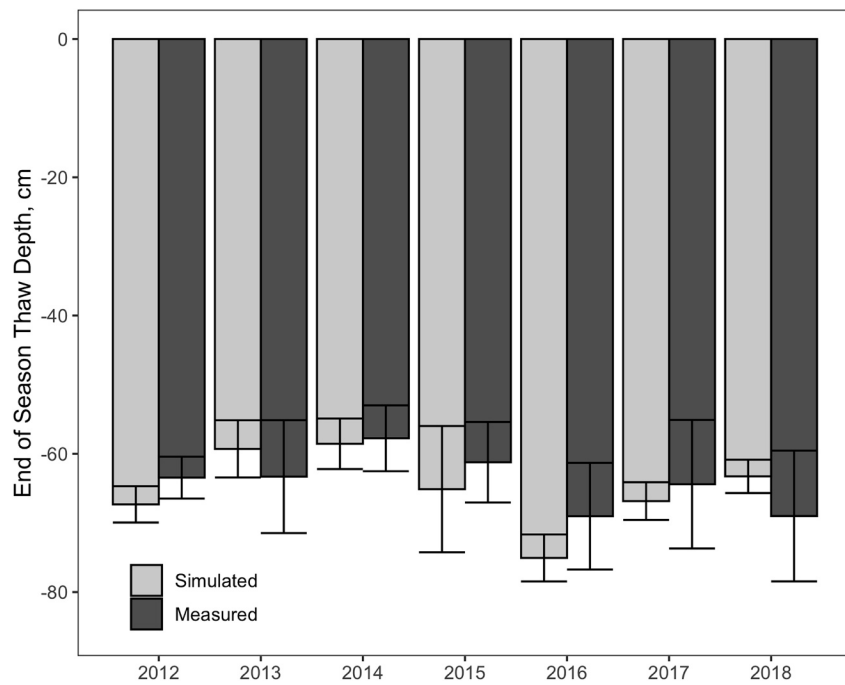
Table 2
Root Mean Square Error (RMSE) and R^2 Between Simulation Median and Corresponding Observed Temperature Time Series, and the Average Overall Interquartile Range for Simulations for Each Corresponding Soil Depth

Variable name	R^2	RMSE	Average IQR
ALT	0.39	4.0	-
5 cm	0.90	1.22	0.51
10 cm	0.78	1.39	0.71
20 cm	0.74	1.01	0.48
40 cm	0.53	0.84	0.36
200 cm	0.02	0.74	0.2
400 cm	0.03	0.53	0.11
800 cm	0.00	0.36	0.04
1500 cm	0.01	0.27	0.01

Note. RMSE and IQR reported in degrees Celsius for each soil layer depth, and cm for active layer thickness (ALT).

Figure 5. End of season thaw depth (cm) over the calibration period. Mean values across measured plots (light gray), and mean values across 500 simulations (dark gray). Error bars correspond to ±1 standard deviation.
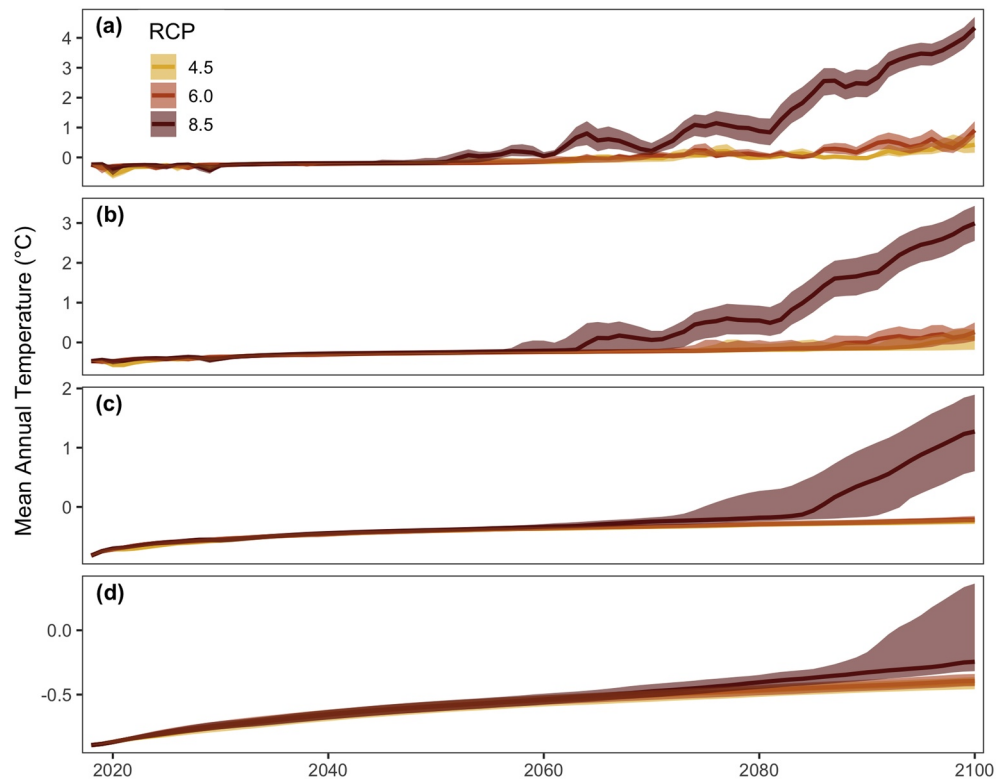

Figure 6. Median annual soil temperatures for select depths of 500 GIPL projections between 2018 and 2100 for different representative climate projections (4.5, 6.0, and 8.5 – yellow, orange, and red solid lines), with shading representing interquartile range. *a–d* correspond to 200, 400, 800, and 1500 cm.
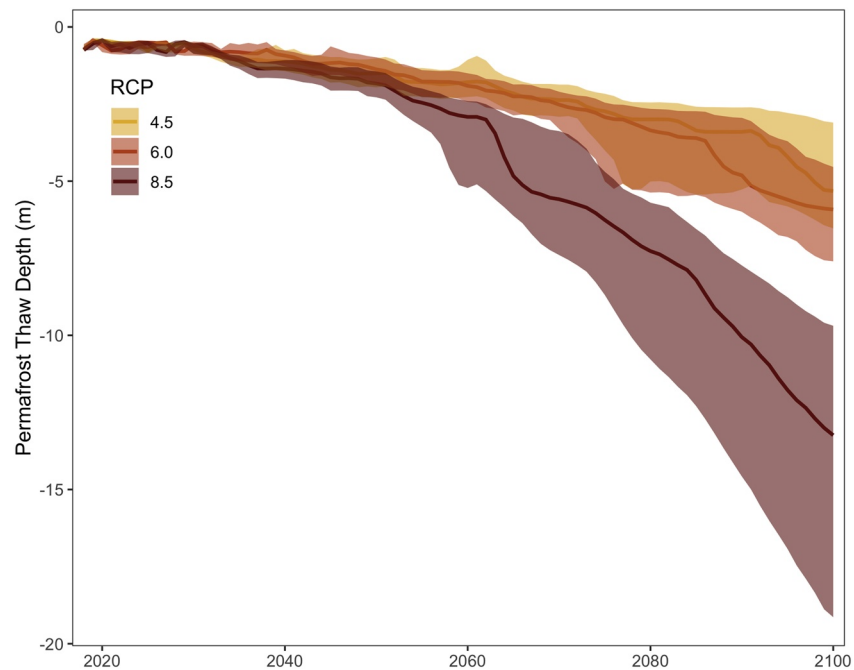
Figure 7. GIPL projections of annual top of Eight Mile Lake permafrost table between 2018a and 2100 for three different representative climate projections (4.5, 6.0, and 8.5 – yellow, orange, and red). Solid line corresponds to median, and shading shows the interquartile range.
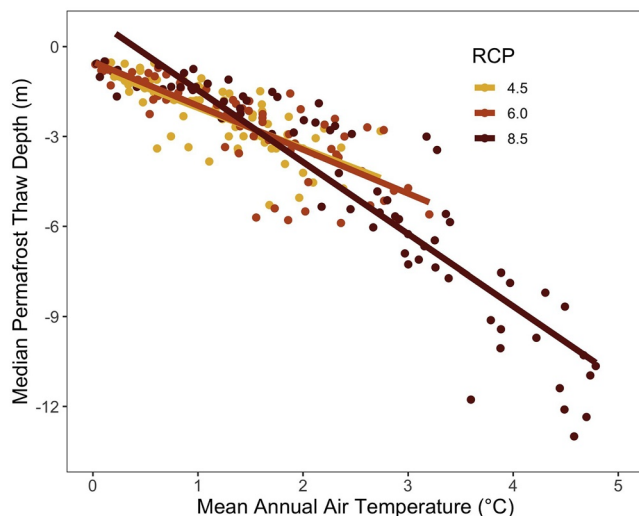

Figure 8. Median permafrost thaw depth (m) and mean annual air temperature for years when values were above the freezing point (*dots*), from 2018 to 2100, and for each representative climate projection (4.5, 6.0, and 8.5 – yellow, orange, and red). Trend lines correspond to best-fit linear model ($p < 0.01$, R^2: 0.52, 0.65, 0.87), demonstrating a range of permafrost thaw rates between 1.35, 1.46, and 2.4 m for every 1 °C warming. Calculated slope terms and associated uncertainty are 1.35 ± 0.16, 1.46 ± 0.13, and 2.4 ± 0.11.

5.3 and 13.2 m depending on the scenario. The IQR for permafrost table position increases as median thaw depth of the permafrost table increases, indicating increasing model uncertainty in projections as thawing proceeds.

The trajectories for permafrost thaw for each concentration pathway demonstrated similar sensitivities to sustained air temperature increase. While mean annual air temperature (MAAT) remained below 0 °C, median permafrost table depth exhibited very little change. In years when MAAT was above 0 °C, there is a strong linear relationship of >1 m thaw per 1 °C of warming for all climate scenarios, after a brief period where permafrost table thawing lagged behind MAAT rise (Figure 8). Calculated slope terms with associated uncertainty are 1.35 ± 0.16, 1.46 ± 0.13, and 2.4 ± 0.11, for RCP 4.5, 6.0, and 8.5, respectively. Our model predicts high vulnerability of the Eight Mile Lake permafrost table to projected increases in air temperature, with high confidence in temperature projections for the upper 800 cm.

We observed similar relationships between projected increases in MAAT and permafrost thaw depth across CMIP5 models. While four of the five models show permafrost thaw projections within close proximity of each other (CCSM4, GISS, IPSL, and MRI) the GFDL model consistently projected deeper permafrost thaw across RCPs (Figure 9). The full range of median permafrost thaw values by 2100 across CMIP5 models were 2.5–15.6 m (RCP 4.5), 2.9–18.3 m (RCP 6.0), and 6.4–24 m (RCP 8.5). Of the five models, only GISS projected median permafrost thaw within the top 3 m by 2100 for RCP 4.5 and 6.0.
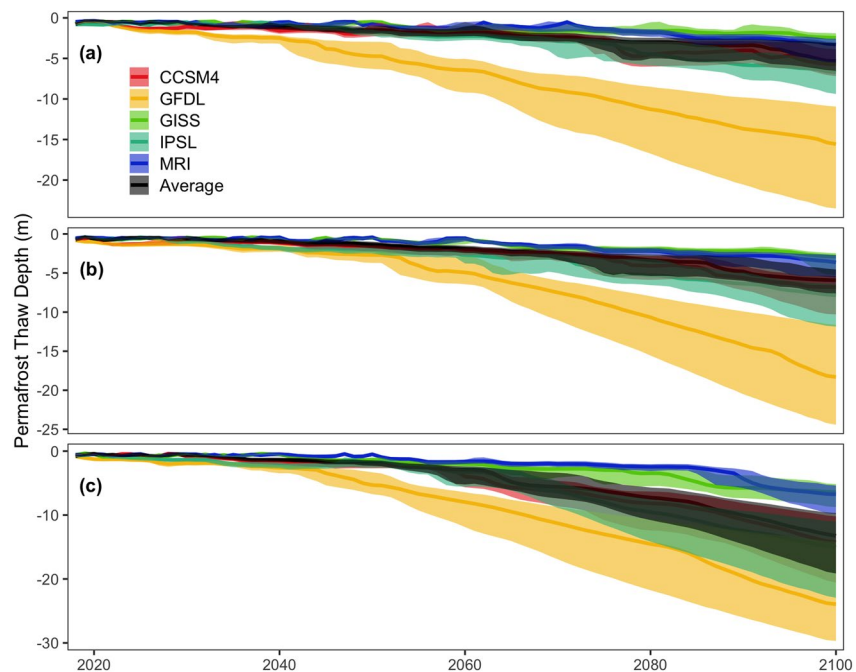
Figure 9. GIPL projections of annual top of Eight Mile Lake permafrost table between 2018 and 2100 for three different representative climate projections (4.5, 6.0, 8.5 – a, b, c), and each of the CMIP5 models (including the 5-Model Average). Solid line corresponds to median, and shading shows the interquartile range.

4. Discussion

Although our model projects permafrost thawing depth is highly dependent on the degree of sustained air warming, none of the projected climate warming scenarios project permafrost in the upper 3 m of soil by 2100. Simulated permafrost thaw began unimpeded at the site once MAAT rose above the freezing point, with peak thaw rate occurring once MAAT warmed past 1°C. Therefore, Eight Mile Lake, as representative of other sub-Arctic tundra areas within the discontinuous permafrost region, will commence significant and uninterrupted permafrost thawing as projected climate warming proceeds. The proximity of sub-Arctic ecosystem MAATs to the freezing point suggest that the onset of irreversible permafrost thawing may occur sooner in some areas than what our simulations projected.

4.1. Eight Mile Lake Permafrost Vulnerability

Our locally calibrated model predicted that Eight Mile Lake permafrost showed high vulnerability to a sustained increase in MAAT, resulting in approximately 1.5 m of permafrost thaw for every 1 °C sustained air warming above 0 °C. However, we suggest that our model may underestimate permafrost thaw based on comparisons to observed thawing and the nature of permafrost temperature responses to lag behind their corresponding air warming trends (Slater & Lawrence, 2013; Zhang et al., 2008). Our results showed a brief lag of permafrost table thawing once MAAT rose above 0 °C, though local environmental variables such as permafrost temperature, organic layer thickness, aboveground plant community, and soil moisture can all affect rates of permafrost temperature response (Chadburn et al., 2017; Fisher et al., 2016; Subin et al., 2013). In context, the Eight Mile Lake research site is located on a gentle slope with historically well-drained soils (E. A. G. Schuur et al., 2007) providing a highly insulative organic layer which protects the permafrost from air temperature rise, suggesting the ability for near surface permafrost to persist through short-term MAAT rise. However, the high permafrost temperatures and relatively shallow moss layer, demonstrated in the model as the top 3 cm layer, may increase site sensitivity.

Given the strong temperature-thaw depth relationship of the site permafrost, the final extent of permafrost thaw depth by 2100 is highly dependent on when site MAAT rises above 0°C. Measured air temperatures at

the site have historically been warmer than comparable downscaled Alaska modeled products (T. Schuur et al., 2020) (Figure S3), suggesting our projections delay permafrost thaw onset. Furthermore, long-term records of deep permafrost temperatures at the Eight Mile Lake site, as well as measured temperatures over the calibration period, demonstrate that permafrost warming occurs at Eight Mile Lake even when MAAT is below 0 °C (Osterkamp & Romanovsky, 1999; Romanovsky et al., 2010). This is also visible from our model projections, which show warming of 1500, 800, 400, and 200 cm layers (Figure 6) well before MAAT crosses the freezing point. Also, recognizing that our model simulated colder deep permafrost temperatures than was measured over the calibration period, we suggest that our projections may further delay the onset of permafrost table deepening.

While most landscape projections of permafrost thaw agree with the pronounced thawing expected to occur across the discontinuous permafrost zone (Chadburn et al., 2017; Guo & Wang, 2016; Hjort et al., 2018; McGuire et al., 2016), results from landscape model ensembles are not always representative of local conditions. In fact, a statewide Alaska GIPL product showed pronounced differences in soil temperature and permafrost table thaw projections for Eight Mile Lake (GIPL Model outputs – linear coupled – Annual. Scenarios Network for Alaska and Arctic Planning) (Figure S4). Our local calibration of soil parameters resulted in a near 30-year delay for thaw of the upper 3 m of permafrost compared with the spatial GIPL product. While the beneficial effect of locally calibrating model parameters is clear, accurately attributing thermodynamic values to soil layers has limited model accessibility. Furthermore, while Arctic soil modeling studies have demonstrated how the inclusion of soil composition (Aalto et al., 2018), deeper layers mineral composition (Alexeev et al., 2007), and latent heat loss reduces model error (Ekici et al., 2015), reliance on coarsely derived values will likely deliver an ill-representative model across heterogeneous permafrost landscapes.

Increased application of local calibration methods will provide researchers valuable comparisons between soil heat modeling of permafrost areas using landscape models. Specifically, exploration of the posterior distributions shown here indicate a sliding influence on temperature between soil thermodynamic parameters through the active layer to latent heat loss terms for permafrost (Figure 3). Such findings can be used to inform parameterization or development efforts of landscape models (Atchley et al., 2015). We found that uncertainty stemming from the parameter distributions contributed to a maximum IQR near 10 m for permafrost thaw projections by 2100 (Figure 7, RCP 8.5), despite only a 4 cm RMSE of seasonal thaw depth over the calibration period. This is in contrast to the disagreement in median Eight Mile Lake permafrost thaw projections across CMIP5 models, which show up to a 16 m difference by 2100 (RCP 8.5), highlighting the relative impact of climate variability and soil thermodynamics to translate into variability in thaw projections. Uncertainty from soil thermal properties are largely ignored in landscape model applications (but see Harp et al., 2015), suggesting that more studies which explore this potential source of uncertainty are needed. With the growing number of Arctic research data repositories (Arctic Permafrost Geospatial Center, NSF Arctic Data Center, NCEAS Arctic Data Center), the potential for application of local model calibration methods is extensive.

4.2. Consequences of Projected Permafrost Thaw

As ice-rich permafrost soils thaw, landscape topography can shift and subside, forming thermokarst features and changing surface water distributions (Belshe et al., 2013; Jorgenson & Osterkamp, 2005). Thermokarst features are often associated with a decline in plant productivity, and a directional change in soil respiration based on the soil moisture conditions (Christensen et al., 2004; Vogel et al., 2009). Therefore, attributing a landscape-scale carbon balance response to increasing permafrost thaw requires tracking the development of subsidence effects and surface soil moisture (Belshe et al., 2012; Mauritz et al., 2017). The upper 1 m of soils at Eight Mile Lake have characteristically high moisture content, within 48%–60% by volume in 2009, which have led to the formation of thermokarst terrain (Osterkamp et al., 2009; Schädel et al., 2018). Topographical subsidence drives a feedback cycle where surface water is redistributed to these lower areas, increasing nonvascular plant coverage and saturating the soil, further driving more subsidence and permafrost thaw. A spatial analysis at a nearby experimental site concluded that surface soil warming of 1 °C was sufficient to initiate thermokarst feature development (Rodenhizer et al., 2020). Furthermore, roughly 1 cm per year of subsidence has

been measured at nearby monitoring plots between 2008 and 2018, though this rate may increase to 5 cm per year as permafrost thaw deepens (Rodenhizer et al., 2020). Thus, we expect that the projected permafrost thawing at Eight Mile Lake will coincide with increased rates of thermokarst feature development and water runoff, which is a dominant mode of ecosystem carbon loss for Tundra ecosystems (Plaza et al., 2019). Projections of between 17 and 21 kg cm^{-2} loss across the Eight Mile Lake watershed by 2100 are expected as permafrost thaw exposes more carbon to decomposition and lateral transport (Plaza et al., 2019; E. A. G. Schuur et al., 2015).

Given the increases in deep soil temperature, active layer depth, permafrost thaw depth, and active layer depth simulated here, we expect that the contribution of soil respiration to the net ecosystem carbon balance to outpace concurrent increases in plant uptake. For well-drained tundra, permafrost thaw can increase plant access to nutrients, such as nitrogen, leading to an increase in carbon uptake and shifts in plant community composition (Aerts et al., 2006; Beermann et al., 2016; Mack et al., 2004; Salmon et al., 2016; Shaver et al., 2007). However, warmed soil and permafrost thaw also stimulate soil respiration (Bracho et al., 2016; Cheng et al., 2017; Natali et al., 2011), which can offset increases growing season carbon uptake through increases in winter soil respiration (Commane et al., 2017; Grogan & Chapin, 1999; Natali et al., 2019; Webb et al., 2016). Measurements of ecosystem carbon balance at Eight Mile Lake demonstrate that this site is an annual source of carbon to the atmosphere (Celis et al., 2017; Trucco et al., 2012), with seasonal active layer thickness and soil temperature strong drivers of GPP and ecosystem respiration (Hicks Pries et al., 2013; Xue et al., 2016). However, changes in plant community composition and surface water distribution do affect soil respiration rates, particularly regarding the shift from CO_2 respiration to methanogenesis in inundated soils (McCalley et al., 2014; Nauta et al., 2014; Taylor et al., 2018). Furthermore, estimates of up to 64% of carbon in the upper half meter of sub-Arctic tundra soil may be lost by 2100 due to hydrological transport alone (Plaza et al., 2019), a process highly influenced by surface permafrost thawing.

The Arctic terrestrial hydrological cycle is tightly coupled with permafrost extent and will likely face dramatic changes as thawing proceeds beyond the upper 3 m. The permafrost layer acts as a boundary for surface water, maintaining the size and continuity of many northern latitude lakes (Bring et al., 2016). Lake waters often expand into degrading permafrost areas, giving the effect of increasing overall lake area, as has been documented throughout the continuous permafrost zone (Smith et al., 2007). Further permafrost thawing can lead to a breach of the lakebed, and the relocation of surface waters underground (Burn, 2005). The namesake body of water near the experimental site, Eight Mile Lake, an ~0.5 km^2 intermediate reservoir along Fish Creek, may face a similar breach-drainage fate by 2100. Drainage of Eight Mile Lake will disrupt river water, nutrient, and mineral outflow around the catchment (Koch et al., 2013), and may lead to a seasonally forming shallow marsh environment with warmer soil layers that facilitate CH_4 respiration. While the reformation of permafrost inside dry lake beds is commonly seen in the continuous permafrost zone, known as the thaw lake cycle (Billings & Peterson, 1980; Britton, 1957), it is unlikely to happen following a MAAT rise above 0°C.

An overall drying of the tundra may occur if permafrost table deepening outpaces surface subsidence in a well-drained soil, as the water table moves further away from the soil surface. Once the seasonal frost layer thaws, any surface water held near the organic layer can drain into groundwater systems (Smith et al., 2005) or topographic depressions, leading to ponding. Increased tundra drying will inhibit nonvascular plant growth, changing above ground carbon storage, and soil heat and water holding potential (Gornall et al., 2007). A combination of increased MAAT and depletion of surface water elevate the risk of higher severity tundra fires (Hu et al., 2010). Post-fire Arctic tundra show increased thermokarst feature development which inhibit landscape recovery (Bret-Harte et al., 2013; Jones et al., 2015), and massive carbon losses from the ecosystem for high severity fires (Mack et al., 2011). However, changes in rooting depth following active layer deepening is known to provide competitive benefits for canopy plant species, potentially paving the way for enhanced Arctic shrubification and increased above-ground carbon storage (Mod & Luoto, 2016). Furthermore, Arctic shrub expansion leads to increases in windblown snow trapping, increasing snowpack depth and further insulating upper soils from cold winter air temperatures (Bring et al., 2016). However the tundra responds to such extensive permafrost thaw, the Eight Mile Lake site is ceded to undergo significant changes by 2100.

5. Conclusions

Using the Bayesian inversion approach with an MCMC technique, we calibrated a permafrost thaw model from local temperature and thaw data, and projected permafrost sensitivity to air warming to 2100 across three climate scenarios. As inferred by the posterior parameter distributions, soil heat capacity and conductance values controlled the temperature response of upper soil layers, while latent heat terms became influential in the permafrost layers. Furthermore, model simulations accurately recreated observed temperature over the calibration period and tightly matched end of season thaw depth. Permafrost at Eight Mile Lake, as representative of other sub-Arctic tundra ecosystems, is extremely vulnerable to projected increases in air temperature, with unimpeded permafrost thaw expected to follow MAAT rise above the freezing point. We found that under no climate scenario was permafrost retained in the upper 3 m of soil. We expect the consequences of such dramatic thawing to include significant soil carbon and nutrient transfer into groundwater, widespread landscape subsidence and thermokarst formation, and an increase in soil respiration of CO_2. An increasing vulnerability of Arctic permafrost to climate warming has hastened the need for site-representative models. Our methodology extends the reach of local calibration efforts, leading to a more detailed understanding of the future of permafrost areas.

Conflict of Interest

The authors declare no conflicts of interest relevant to this study.

Data Availability Statement

Eight Mile Lake climate and soil temperature and thaw depth data can be retrieved online from the Bonanza Creek Long Term Experimental Research repository (https://www.lter.uaf.edu/). Datasets for this research are available in these in-text data citation references: Celis et al. (2019), Celis et al. (2016), Kelley et al. (2019), Ledman et al. (2018). All data are archived in the Bonanza Creek LTER Data Catalog and at Ameriflux. An annotated copy of the Bayesian Model Framework code can be found in a Zenodo repository (https://doi.org/10.5281/zenodo.4374125 (Garnello, 2020)).

References

Aalto, J., Karjalainen, O., Hjort, J., & Luoto, M. (2018). Statistical forecasting of current and future circum-Arctic ground temperatures and active layer thickness. *Geophysical Research Letters*, *45*(10), 4889–4898. https://doi.org/10.1029/2018GL078007

Aerts, R., Cornelissen, J. H. C., & Dorrepaal, E. (2006). Plant performance in a warmer world: General responses of plants from cold, northern biomes and the importance of winter and spring events. *Plant Ecology*, *182*(1–2), 65–77. https://doi.org/10.1007/s11258-005-9031-1

Åkerman, H. J., & Johansson, M. (2008). Thawing permafrost and thicker active layers in sub-arctic Sweden. *Permafrost and Periglacial Processes*, *19*(3), 279–292. https://doi.org/10.1002/ppp.626

Alexeev, V. A., Nicolsky, D. J., Romanovsky, V. E., & Lawrence, D. M. (2007). An evaluation of deep soil configurations in the CLM3 for improved representation of permafrost. *Geophysical Research Letters*, *34*(9), 1–5. https://doi.org/10.1029/2007GL029536

Andersen, K. E., Brooks, S. P., & Hansen, M. B. (2003). Bayesian inversion of geoelectrical resistivity data. *Journal of the Royal Statistical Society: Series B (Statistical Methodology)*, *65*(3), 619–642. https://doi.org/10.1111/1467-9868.00406

Atchley, A. L., Painter, S. L., Harp, D. R., Coon, E. T., Wilson, C. J., Liljedahl, A. K., & Romanovsky, V. E. (2015). Using field observations to inform thermal hydrology models of permafrost dynamics with ATS (v0.83). *Geoscientific Model Development*, *8*(9), 2701–2722. https://doi.org/10.5194/gmd-8-2701-2015

Beermann, F., Langer, M., Wetterich, S., Strauss, J., Boike, J., Schirrmeister, L., et al. (2016). Permafrost thaw and release of inorganic nitrogen from polygonal tundra soils in eastern Siberia. *Biogeosciences Discussions*(April), 1–27. https://doi.org/10.5194/bg-2016-117

Belshe, E. F., Schuur, E. A. G., Bolker, B. M., & Bracho, R. (2012). Incorporating spatial heterogeneity created by permafrost thaw into a landscape carbon estimate. *Journal of Geophysical Research: Biogeosciences*, *117*(1), 1–14. https://doi.org/10.1029/2011JG001836

Belshe, E. F., Schuur, E. A. G., & Grosse, G. (2013). Quantification of upland thermokarst features with high resolution remote sensing. *Environmental Research Letters*, *8*(3). https://doi.org/10.1088/1748-9326/8/3/035016

Beven, K., & Freer, J. (2001). Equifinality, data assimilation, and uncertainty estimation in mechanistic modeling of complex environmental systems using the GLUE methodology. *Journal of Hydrology*, *249*, 11–29. https://doi.org/10.1524/anly.2006.26.99.365

Billings, W. D., & Peterson, K. M. (1980). Vegetational change and ice-wedge polygons through the thaw-lake cycle in arctic Alaska. *Arctic & Alpine Research*, *12*(4), 413–432. https://doi.org/10.2307/1550492

Bracho, R., Natali, S., Pegoraro, E., Crummer, K. G., Schädel, C., Celis, G., et al. (2016). Temperature sensitivity of organic matter decomposition of permafrost-region soils during laboratory incubations. *Soil Biology and Biochemistry*, *97*, 1–14. https://doi.org/10.1016/j.soilbio.2016.02.008

Bret-Harte, M. S., Mack, M. C., Shaver, G. R., Huebner, D. C., Johnston, M., Mojica, C. A., et al. (2013). The response of Arctic vegetation and soils following an unusually severe tundra fire. *Philosophical Transactions of the Royal Society B: Biological Sciences*, *368*(1624). https://doi.org/10.1098/rstb.2012.0490

Bring, A., Fedorova, I., Dibike, Y., Hinzman, L., Mård, J., Mernild, S. H., et al. (2016). Arctic terrestrial hydrology: A synthesis of processes, regional effects, and research challenges. *Journal of Geophysical Research G: Biogeosciences*, *121*(3), 621–649. https://doi.org/10.1002/2015JG003131

Britton, M. E. (1957). In H. P. Hanson (Ed.), *Vegetation of the arctic tundra* (2nd ed.). Corvallis: Oregon State Chapter of Phi Kappa Phi, Oregon State College.

Brown, R. D., Brasnett, B., & Robinson, D. (2003). Gridded North American monthly snow depth and snow water equivalent for GCM evaluation. *Atmosphere-Ocean*, *41*(1), 1–14. https://doi.org/10.3137/ao.410101

Burn, C. R. (2005). Lake-bottom thermal regimes, western Arctic Coast, Canada. *Permafrost and Periglacial Processes*, *16*(4), 355–367. https://doi.org/10.1002/ppp.542

Cavallaro, N., Shrestha, G., Birdsey, R., Mayes, M. A., Najjar, R. G., Reed, S. C., et al. (2018). *Second State of the Carbon Cycle Report (SOC-CR2): A sustained assessment report*. Washington, DC: USGCRP. https://doi.org/10.7930/Soccr2.2018

Celis, G., Bracho, R., & Schuur, T. (2016). Eight Mile Lake Research Watershed, thaw gradient: CO2 fluxes eddy covariance 2008–2015. Bonanza Creek LTER - University of Alaska Fairbanks. Retrieved from http://www.lter.uaf.edu/data/data-detail/id/642

Celis, G., Ledman, J., Bracho, R., & Schuur, T. (2019). Eight Mile Lake Research Watershed, thaw gradient half-hourly soil temperature 2004–2018. Bonanza Creek LTER - University of Alaska Fairbanks. https://doi.org/10.6073/pasta/29d79cf984929bc247173268c3785eca

Celis, G., Mauritz, M., Bracho, R., Salmon, V. G., Webb, E. E., Hutchings, J. A., et al. (2017). Tundra is a consistent source of CO_2 at a site with progressive permafrost thaw during 6 years of chamber and eddy covariance measurements. *Journal of Geophysical Research: Biogeosciences*, *122*, 1–15. https://doi.org/10.1002/2017JD02715710.1002/2016jg003671

Chadburn, S. E., Burke, E. J., Cox, P. M., Friedlingstein, P., Hugelius, G., & Westermann, S. (2017). An observation-based constraint on permafrost loss as a function of global warming. *Nature Climate Change*, *7*(5), 340–344. https://doi.org/10.1038/nclimate3262

Cheng, L., Zhang, N., Yuan, M., Xiao, J., Qin, Y., Deng, Y., et al. (2017). Warming enhances old organic carbon decomposition through altering functional microbial communities. *The ISME Journal*, *11*(8), 1–11. https://doi.org/10.1038/ismej.2017.48

Christensen, T. R., Johansson, T., Jonas Åkerman, H., Mastepanov, M., Malmer, N., Friborg, T., et al. (2004). Thawing sub-arctic permafrost: Effects on vegetation and methane emissions. *Geophysical Research Letters*, *31*(4), L04501. https://doi.org/10.1029/2003GL018680

Commane, R., Lindaas, J., Benmergui, J., Luus, K. A., Chang, R. Y.-W., Daube, B. C., et al. (2017). Carbon dioxide sources from Alaska driven by increasing early winter respiration from Arctic tundra. *Proceedings of the National Academy of Sciences*, *114*(21), 5361–5366. https://doi.org/10.1073/pnas.1618567114

Daly, C., Gibson, W. P., Taylor, G. H., Johnson, G. L., & Pasteris, P. (2002). A knowledge-based approach to the statistical mapping of climate. *Climate Research*, *22*(2), 99–113. https://doi.org/10.3354/cr022099

Davidson, E. A., & Janssens, I. A. (2006). Temperature sensitivity of soil carbon decomposition and feedbacks to climate change. *Nature*. https://doi.org/10.1038/nature04514

Ekici, A., Chadburn, S., Chaudhary, N., Hajdu, L. H., Marmy, A., Peng, S., et al. (2015). Site-level model intercomparison of high latitude and high altitude soil thermal dynamics in tundra and barren landscapes. *The Cryosphere*, *9*(4), 1343–1361. https://doi.org/10.5194/tc-9-1343-2015

Farouki, O. T. (1981). Thermal properties of soils. CRREL Monograph (US Army Cold Regions Research and Engineering Laboratory). https://doi.org/10.21236/ada111734

Fisher, J. P., Estop-Aragonés, C., Thierry, A., Charman, D. J., Wolfe, S. A., Hartley, I. P., et al. (2016). The influence of vegetation and soil characteristics on active-layer thickness of permafrost soils in boreal forest. *Global Change Biology*, *22*(9), 3127–3140. https://doi.org/10.1111/gcb.13248

Garnello, A. (2020). *Bayesian framework for GIPL parameter estimation*. Zenodo. https://doi.org/10.5281/zenodo.4374125

Gelman, A., & Rubin, B. D. (1992). Inference from iterative simulation using multiple sequences. *Statistical Science*, *7*(4), 457–511. https://doi.org/10.2307/2246134

GIPL Model outputs - linear coupled - Annual. (n.d.). Retrieved from http://ckan.snap.uaf.edu/dataset/gipl-model-outputs-linear-coupled-annual

Gornall, J. L., Jónsdóttir, I. S., Woodin, S. J., & Van Der Wal, R. (2007). Arctic mosses govern below-ground environment and ecosystem processes. *Oecologia*, *153*(4), 931–941. https://doi.org/10.1007/s00442-007-0785-0

Grogan, P., & Chapin, F. S. (1999). Arctic soil respiration: Effects of climate and vegetation depend on season. *Ecosystems*, *2*(5), 451–459. https://doi.org/10.1007/s100219900093

Guo, D., & Wang, H. (2016). CMIP5 permafrost degradation projection: A comparison among different regions. *Journal of Geophysical Research: Atmospheres*, *175*(4449), 238. https://doi.org/10.1038/175238c0

Harp, D. R., Atchley, A. L., Painter, S. L., Coon, E. T., Wilson, C. J., Romanovsky, V. E., & Rowland, J. C. (2015). Effect of soil property uncertainties on permafrost thaw projections: A calibration-constrained analysis. *The Cryosphere Discussions*, *9*(3), 3351–3404. https://doi.org/10.5194/tcd-9-3351-2015

Hicks Pries, C. E., Schuur, E. A. G., & Crummer, K. G. (2013). Thawing permafrost increases old soil and autotrophic respiration in tundra: Partitioning ecosystem respiration using δ13C and Δ14C. *Global Change Biology*, *19*(2), 649–661. https://doi.org/10.1111/gcb.12058

Hjort, J., Karjalainen, O., Aalto, J., Westermann, S., Romanovsky, V. E., Nelson, F. E., et al. (2018). Degrading permafrost puts Arctic infrastructure at risk by mid-century. *Nature Communications*, *9*(1). https://doi.org/10.1038/s41467-018-07557-4

Hu, F. S., Higuera, P. E., Walsh, J. E., Chapman, W. L., Duffy, P. A., Brubaker, L. B., & Chipman, M. L. (2010). Tundra burning in Alaska: Linkages to climatic change and sea ice retreat. *Journal of Geophysical Research: Biogeosciences*, *115*(4), 1–8. https://doi.org/10.1029/2009JG001270

Jafarov, E. E., Marchenko, S. S., & Romanovsky, V. E. (2012). Numerical modeling of permafrost dynamics in Alaska using a high spatial resolution dataset. *The Cryosphere*, *6*(3), 613–624. https://doi.org/10.5194/tc-6-613-2012

Jones, B. M., Larsen, C. F., Hayes, D. J., Liu, L., Miller, E., Grosse, G., & Arp, C. D. (2015). Recent Arctic tundra fire initiates widespread thermokarst development. *Scientific Reports*, *5*(1), 1–13. https://doi.org/10.1038/srep15865

Jorgenson, M. T., Romanovsky, V., Harden, J., Shur, Y., O'Donnell, J., Schuur, E. A. G., et al. (2010). Resilience and vulnerability of permafrost to climate change. *Canadian Journal of Forest Research*, *40*(7), 1219–1236. https://doi.org/10.1139/X10-060

Jorgenson, T., & Osterkamp, T. (2005). Response of boreal ecosystems to varying modes of permafrost degradation. *Canadian Journal of Forest Research*, *35*(9), 2100–2111. https://doi.org/10.1139/x05-153

Kelley, A., Pegoraro, E., Mauritz, M., Hutchings, J., Natali, S., & Hicks-Pries, C. (2019). Eight Mile Lake Research watershed, thaw gradient: Seasonal thaw depth 2004–2019. Bonanza Creek LTER - University of Alaska Fairbanks. https://doi.org/10.6073/pasta/86617226553d16413ac6e70073bfc4a8

Kersten, M. (1949). Thermal properties of soils and rocks. *Bulletin 28. University of Minnesota, Engineering Experiment Station*, *52*(21), 310.

Keuper, F., van Bodegom, P. M., Dorrepaal, E., Weedon, J. T., van Hal, J., van Logtestijn, R. S. P., & Aerts, R. (2012). A frozen feast: Thawing permafrost increases plant-available nitrogen in subarctic peatlands. *Global Change Biology*, *18*(6), 1998–2007. https://doi.org/10.1111/j.1365-2486.2012.02663.x

Koch, J. C., Runkel, R. L., Striegl, R., & McKnight, D. M. (2013). Hydrologic controls on the transport and cycling of carbon and nitrogen in a boreal catchment underlain by continuous permafrost. *Journal of Geophysical Research: Biogeosciences*, *118*(2), 698–712. https://doi.org/10.1002/jgrg.20058

Koven, C. D., Riley, W. J., & Stern, A. (2013). Analysis of permafrost thermal dynamics and response to climate change in the CMIP5 earth system models. *Journal of Climate*, *26*(6), 1877–1900. https://doi.org/10.1175/JCLI-D-12-00228.1

Ledman, J., Schuur, T., & Mauritz, M. (2018). *Eight Mile Lake Research watershed, thaw gradient: Half-hourly snow depth data 2012–2017*. Bonanza Creek LTER - University of Alaska Fairbanks. https://doi.org/10.6073/pasta/50343ecc90b137f4713e4952b292d655

Littell, J. S., McAfee, S. A., Hayward, G. D., Littell, J. S., McAfee, S. A., & Hayward, G. D. (2018). Alaska snowpack response to climate change: Statewide snowfall equivalent and snowpack water scenarios. *Water*, *10*(5), 668. https://doi.org/10.3390/w10050668

Luo, Y., & Schuur, E. A. G. (2020). Model parameterization to represent processes at unresolved scales and changing properties of evolving systems. *Global Change Biology*, *26*(3), 1109–1117. https://doi.org/10.1111/gcb.14939

Mack, M. C., Bret-Harte, M. S., Hollingsworth, T. N., Jandt, R. R., Schuur, E. A. G., Shaver, G. R., & Verbyla, D. L. (2011). Carbon loss from an unprecedented Arctic tundra wildfire. *Nature*, *475*(7357), 489–492. https://doi.org/10.1038/nature10283

Mack, M. C., Schuur, E. A. G., Bret-Harte, M. S., Shaver, G. R., & Chapin, F. S. (2004). Ecosystem carbon storage in arctic tundra reduce by long-term nutrient fertilization. *Nature*, *431*(7007), 440–443. https://doi.org/10.1038/nature02887

Marchenko, S., Romanovsky, V., & Tipenko, G. (2008). Numerical modeling of spatial permafrost dynamics in Alaska. *Proceedings of the ninth international conference on permafrost, 0–5*. Retrieved from http://www.lter.uaf.edu/pdf/1308_Marchenko_Romanovsky_2008.pdf

Mauritz, M., Bracho, R., Celis, G., Hutchings, J., Natali, S. M., Pegoraro, E., et al. (2017). Nonlinear CO_2 flux response to 7 years of experimentally induced permafrost thaw. *Global Change Biology*, 3646–3666. https://doi.org/10.1111/gcb.13661

McCalley, C. K., Woodcroft, B. J., Hodgkins, S. B., Wehr, R. A., Kim, E.-H., Mondav, R., et al. (2014). Methane dynamics regulated by microbial community response to permafrost thaw. *Nature*, *514*(7523), 478–481. https://doi.org/10.1038/nature13798

McGuire, A. D., Koven, C., Lawrence, D. M., Clein, J. S., Xia, J., Beer, C., et al. (2016). Variability in the sensitivity among model simulations of permafrost and carbon dynamics in the permafrost region between 1960 and 2009. *Global Biogeochemical Cycles*, *30*, 1015–1037. https://doi.org/10.1002/2016GB005405

Metropolis, N., Rosenbluth, A. W., Rosenbluth, M. N., Teller, A. H., & Teller, E. (1953). Equation of state calculation by fast computing machines. *The Journal of Chemical Physics*, *21*(6), 1087–1092. https://doi.org/10.1063/1.1699114

Mod, H., & Luoto, M. (2016). Arctic shrubification mediates the impacts of warming climate on changes to tundra vegetation. *Environmental Research Letters*, *11*. https://doi.org/10.1088/1748-9326/11/12/124028

Natali, S. M., Schuur, E. A. G., Trucco, C., Hicks Pries, C. E., Crummer, K. G., & Baron Lopez, A. F. (2011). Effects of experimental warming of air, soil and permafrost on carbon balance in Alaskan tundra. *Global Change Biology*, *17*(3), 1394–1407. https://doi.org/10.1111/j.1365-2486.2010.02303.x

Natali, S. M., Watts, J. D., Rogers, B. M., Potter, S., Ludwig, S. M., Selbmann, A. K., et al. (2019). Large loss of CO_2 in winter observed across the northern permafrost region. *Nature Climate Change*, *9*(11), 852–857. https://doi.org/10.1038/s41558-019-0592-8

Nauta, A. L., Heijmans, M. M. P. D., Blok, D., Limpens, J., Elberling, B., Gallagher, A., et al. (2014). Permafrost collapse after shrub removal shifts tundra ecosystem to a methane source. *Nature Climate Change*, *5*, 67. https://doi.org/10.1038/nclimate2446

Nicolsky, D., Romanovsky, V., & Panteleev, G. (2009). Estimation of soil thermal properties using in-situ temperature measurements in the active layer and permafrost. *Cold Regions Science and Technology*, *55*(1), 120–129. https://doi.org/10.1016/j.coldregions.2008.03.003

Nicolsky, D., Romanovsky, V., & Tipenko, G. (2007). Using in-situ temperature measurements to estimate saturated soil thermal properties by solving a sequence of optimization problems. *The Cryosphere*, *1*(1), 41–58. https://doi.org/10.5194/tc-1-41-2007

Olefeldt, D., Goswami, S., Grosse, G., Hayes, D., Hugelius, G., Kuhry, P., et al. (2016). Circumpolar distribution and carbon storage of thermokarst landscapes. *Nature Communications*, *7*, 1–11. https://doi.org/10.1038/ncomms13043

Osterkamp, T., Jorgenson, T., Schuur, E., Shur, Y., Kanevskiy, M., Vogel, J., & Tumskoy, V. (2009). Physical and ecological changes associated with warming permafrost and thermokarst in interior Alaska. *Permafrost and Periglacial Processes*, *20*, 235–256. https://doi.org/10.1002/ppp10.1002/ppp.656

Osterkamp, T., & Romanovsky, V. (1999). Evidence for warming and thawing of discontinuous permafrost in Alaska. *Permafrost and Periglacial Processes*, *10*(1), 17–37. https://doi.org/10.1002/(SICI)1099-1530(199901/03)10:1<17::AID-PPP303>3.0.CO;2-4

Parmentier, F. J. W., Christensen, T. R., Rysgaard, S., Bendtsen, J., Glud, R. N., Else, B., et al. (2017). A synthesis of the arctic terrestrial and marine carbon cycles under pressure from a dwindling cryosphere. *Ambio*, *46*(s1), 53–69. https://doi.org/10.1007/s13280-016-0872-8

Pastick, N. J., Jorgenson, M. T., Wylie, B. K., Nield, S. J., Johnson, K. D., & Finley, A. O. (2015). Distribution of near-surface permafrost in Alaska: Estimates of present and future conditions. *Remote Sensing of Environment*, *168*, 301–315. https://doi.org/10.1016/j.rse.2015.07.019

Plaza, C., Pegoraro, E., Bracho, R., Celis, G., Crummer, K. G., Hutchings, J. A., et al. (2019). Direct observation of permafrost degradation and rapid soil carbon loss in tundra. *Nature Geoscience*, *12*(8), 627–631. https://doi.org/10.1038/s41561-019-0387-6

Plummer, M., Best, N., Cowles, K., & Vines, K. (2006). CODA: Convergence diagnosis and output analysis for MCMC. *R News*, *6*, 7–11.

Pries, C. E. H., Schuur, E. A. G., & Crummer, K. G. (2012). Holocene carbon stocks and carbon accumulation rates altered in soils undergoing permafrost thaw. *Ecosystems*, *15*, 162–173. https://doi.org/10.1007/s10021-011-9500-4

R Core Team. (2019). R: A language and environment for statistical computing. *Journal of Chemical Information and Modeling*. Vienna, Austria: R Foundation for Statistical Computing. https://doi.org/10.1017/CBO9781107415324.004

Rodenhizer, H., Ledman, J., Mauritz, M., Natali, S. M., Pegoraro, E., Plaza, C., et al. (2020). Carbon thaw rate doubles when accounting for subsidence in a permafrost warming experiment. *Journal of Geophysical Research: Biogeosciences*, *125*, 1–16. https://doi.org/10.1029/2019jg005528

Romanovsky, V., Isaksen, K., Drozdov, D., Anisimov, O., Instanes, A., Leibman, M., et al. (2017). [Changing permafrost and its impacts]. In *Snow, water, ice and permafrost in the arctic (SWIPA)*. Oslow, Norway: Narayana Press.

Romanovsky, V., Kholodov, A., Marchenko, S., Oberman, N., Drozdov, D., Malkova, G., et al. (2008). *Thermal state and fate of permafrost in Russia: First results of IPY* (Vol. 29, pp. 1511–1518). Retrieved from www.onsetcomp.com/

Romanovsky, V., & Osterkamp, T. (2000). Effects of unfrozen water on heat and mass transport processes in the active layer and permafrost. *Permafrost and Periglacial Processes*, *11*(3), 219–239. https://doi.org/10.1002/1099-1530(200007/09)11:3<219::AID-PPP352>3.0.CO;2-7

Romanovsky, V., Sazonova, T. S., Balobaev, V. T., Shender, N. I., & Sergueev, D. O. (2007). Past and recent changes in air and permafrost temperatures in eastern Siberia. *Global and Planetary Change*, *56*(3), 399–413. https://doi.org/10.1016/j.gloplacha.2006.07.022

Romanovsky, V., Smith, S., & Christiansen, H. (2010). Permafrost thermal state in the polar northern hemisphere during the international polar year 2007–2009: A synthesis. *Permafrost and Periglacial Processes*, *21*(2), 106–116. https://doi.org/10.1002/ppp.689

Romanovsky, V., Smith, S. L., Isaksen, K., Nyland, K. E., Kholodov, A. L., Shiklomanov, N. I., et al. (2020). *Terrestrial permafrost. State of the climate 2019*.

Salmon, V. G., Soucy, P., Mauritz, M., Celis, G., Natali, S. M., Mack, M. C., & Schuur, E. A. G. (2016). Nitrogen availability increases in a tundra ecosystem during five years of experimental permafrost thaw. *Global Change Biology*, *22*(5), 1927–1941. https://doi.org/10.1111/gcb.13204

Schädel, C., Koven, C., Lawrence, D. M., Celis, G., Garnello, A. J., Hutchings, J., et al. (2018). Divergent patterns of experimental and model-derived permafrost ecosystem carbon dynamics in response to Arctic warming. *Environmental Research Letters*, *13*(10), 0–18. https://doi.org/10.1088/1748-9326/aae0ff

Schuur, E. A. G., Bockheim, J., Canadell, J. G., Euskirchen, E., Field, C. B., Goryachkin, S. V., et al. (2008). Vulnerability of permafrost carbon to climate change: Implications for the global carbon cycle. *BioScience*, *58*(8), 701. https://doi.org/10.1641/B580807

Schuur, E. A. G., Crummer, K. G., Vogel, J. G., & Mack, M. C. (2007). Plant species composition and productivity following permafrost thaw and thermokarst in Alaskan tundra. *Ecosystems*, *10*, 280–292. https://doi.org/10.1007/s10021-007-9024-0

Schuur, E. A. G., Mcguire, A. D., Schädel, C., Grosse, G., Harden, J. W., Hayes, D. J., et al. (2015). Climate change and the permafrost carbon feedback. *Nature*. https://doi.org/10.1038/nature14338

Schuur, E. A. G., Vogel, J. G., Crummer, K. G., Lee, H., Sickman, J. O., & Osterkamp, T. E. (2009). The effect of permafrost thaw on old carbon release and net carbon exchange from tundra. *Nature*, *459*(7246), 556–559. https://doi.org/10.1038/nature08031

Schuur, T., Bracho, R., & Celis, G. (2020). Fifteen years of carbon exchange dynamics reveals tundra to be a persistent source of carbon to the atmosphere where permafrost is degrading. *Journal of Geophysical Research: Biogeosciences*.

Serreze, M. C., Walsh, J. E., Chapin, F. S., Osterkamp, T., Dyurgerov, M., Romanovsky, V., et al. (2000). Observational evidence of recent change in the northern high-latitude environment. *Climatic Change*, *46*(1), 159–207. https://doi.org/10.1023/A:1005504031923

Shaver, G. R., Street, L. E., Rastetter, E. B., VanWijk, M. T., & Williams, M. (2007). Functional convergence in regulation of net CO_2 flux in heterogeneous tundra landscapes in Alaska and Sweden. *Journal of Ecology*, *95*(4), 802–817. https://doi.org/10.1111/j.1365-2745.2007.01259.x

Shur, Y., & Jorgenson, M. T. (2007). Patterns of permafrost formation and degradation in relation to climate and ecosystems. *Permafrost and Periglacial Processes*, *18*, 7–19. https://doi.org/10.1002/ppp10.1002/ppp.582

Slater, A. G., & Lawrence, D. M. (2013). Diagnosing present and future permafrost from climate models. *Journal of Climate*, *26*(15), 5608–5623. https://doi.org/10.1175/JCLI-D-12-00341.1

Smith, L. C., Pavelsky, T. M., MacDonald, G. M., Shiklomanov, A. I., & Lammers, R. B. (2007). Rising minimum daily flows in northern Eurasian rivers: A growing influence of groundwater in the high-latitude hydrologic cycle. *Journal of Geophysical Research: Biogeosciences*, *112*(4). https://doi.org/10.1029/2006JG000327

Smith, L. C., Sheng, Y., MacDonald, G. M., & Hinzman, L. D. (2005). Atmospheric science: Disappearing Arctic lakes. *Science*, *308*(5727), 1429. https://doi.org/10.1126/science.1108142

Spall, C. J. (2003). In R. Graham, J. K. Lenstra, & J. Spencer (Eds.), *Introduction to stochastic search and optimization: Estimation, simulation*. Hoboken, New Jersey: Wiley-Interscience Series in Discrete Mathematics and Optimization. https://doi.org/10.1002/0471722138

Subin, Z. M., Koven, C. D., Riley, W. J., Torn, M. S., Lawrence, D. M., & Swenson, S. C. (2013). Effects of soil moisture on the responses of soil temperatures to climate change in cold regions. *Journal of Climate*, *26*(10), 3139–3158. https://doi.org/10.1175/JCLI-D-12-00305.1

Tarnocai, C., Canadell, J. G., Schuur, E. A. G., Kuhry, P., Mazhitova, G., & Zimov, S. (2009). Soil organic carbon pools in the northern circumpolar permafrost region. *Global Biogeochemical Cycles*, *23*(2). https://doi.org/10.1029/2008GB003327

Taylor, M. A., Celis, G., Ledman, J. D., Bracho, R., & Schuur, E. A. G. (2018). Methane efflux measured by eddy covariance in Alaskan upland tundra undergoing permafrost degradation. *Journal of Geophysical Research: Biogeosciences*, *123*(9), 2695–2710. https://doi.org/10.1029/2018JG004444

Trucco, C., Schuur, E. A. G., Natali, S. M., Belshe, E. F., Bracho, R., & Vogel, J. (2012). Seven-year trends of CO_2 exchange in a tundra ecosystem affected by long-term permafrost thaw. *Journal of Geophysical Research: Biogeosciences*, *117*(2), 1–12. https://doi.org/10.1029/2011JG001907

van Huissteden, J., & Dolman, A. (2012). Soil carbon in the Arctic and the permafrost carbon feedback. *Current Opinion in Environmental Sustainability*, *4*(5), 545–551. https://doi.org/10.1016/J.COSUST.2012.09.008

Verseghy, D. L. (1991). CLASS – A Canadian land surface scheme for GCMs. *International Journal of Climatology*, *11*, 111–133.

Vogel, J., Schuur, E. A. G., Trucco, C., & Lee, H. (2009). Response of CO_2 exchange in a tussock tundra ecosystem to permafrost thaw and thermokarst development. *Journal of Geophysical Research*, *114*, G04018. https://doi.org/10.1029/2008JG000901

Webb, E. E., Schuur, E. A. G., Natali, S. M., Oken, K. L., Bracho, R., Krapek, J. P., et al. (2016). Increased wintertime CO_2 loss as a result of sustained tundra warming. *Journal of Geophysical Research: Biogeosciences*, 249–265. https://doi.org/10.1002/2014JG002795

Xu, T., White, L., Hui, D., & Luo, Y. (2006). Probabilistic inversion of a terrestrial ecosystem model: Analysis of uncertainty in parameter estimation and model prediction. *Global Biogeochemical Cycles*, *20*(2), 1–15. https://doi.org/10.1029/2005GB002468

Xue, K., Yuan, M., Shi, M. J. Z., Qin, Y., Deng, Y., Cheng, L., et al. (2016). Tundra soil carbon is vulnerable to rapid microbial decomposition under climate warming. *Nature Climate Change*, *6*(6), 595–600. https://doi.org/10.1038/nclimate2940

Zhang, Y., Chen, W., & Riseborough, D. W. (2008). Disequilibrium response of permafrost thaw to climate warming in Canada over 1850–2100. *Geophysical Research Letters*, *35*(2), L02502. https://doi.org/10.1029/2007GL032117

Zhu, D., Ciais, P., Krinner, G., Maignan, F., Jornet Puig, A., & Hugelius, G. (2019). Controls of soil organic matter on soil thermal dynamics in the northern high latitudes. *Nature Communications*, *10*(1). https://doi.org/10.1038/s41467-019-11103-1